Open Access
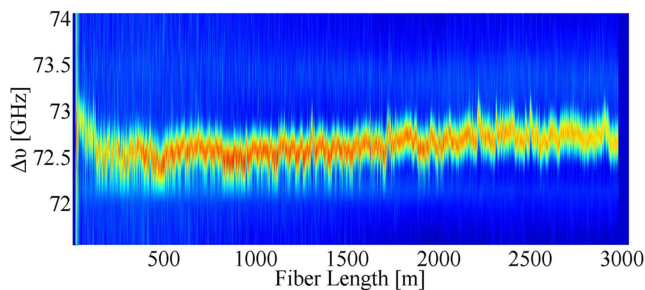
Distributed Birefringence Measurement of a Polarization-Maintaining Fiber With an Extended Range Based on an Enhanced Brillouin Dynamic Grating

Taofei Jiang
Dengwang Zhou
Meng Xia
Lei Teng
Dexin Ba
Yongkang Dong, *Member, IEEE*

Distributed Birefringence Measurement of a Polarization-Maintaining Fiber With an Extended Range Based on an Enhanced Brillouin Dynamic Grating

Taofei Jiang ⓘ **, Dengwang Zhou** ⓘ **, Meng Xia, Lei Teng, Dexin Ba, and Yongkang Dong** ⓘ **,** *Member, IEEE*

National key Laboratory of Science and Technology on Tunable Laser, Harbin Institute of Technology, Harbin 150001, China

Abstract: A distributed birefringence measurement of a polarization-maintaining fiber (PMF) can be realized by using a Brillouin dynamic grating (BDG). However, the pump depletion decreases the intensity of the BDG along the PMF and limits the measurement range to a few hundred meters. We demonstrate a distributed birefringence measurement of the PMF with an extended range to 3030 m based on an enhanced BDG with an 18.5-ns pump-1 pulse, frequency-upshifted continuous-wave pump-2, and 4-ns read pulse (spatial resolution: 40 cm). The enhanced BDG is promising to characterize the design of a fiber coil to improve the fiber optic gyroscope performance.

Index Terms: Brillouin optical fiber sensor, Brillouin dynamic grating, birefringence measurement, polarization maintaining fiber.

1. Introduction

Since the Brillouin dynamic grating (BDG) in a polarization-maintaining fiber (PMF) was proposed in 2008 [1], extensive studies have been carried out on its fundamental properties [2]–[3] and potential applications, such as all-optical calculus [4], fiber sensing [5]–[9], high-resolution optical spectrometry [10], tunable optical delays [11], distributed birefringence measurement [12]–[13], ultra-wideband communications [14] and microwave-photonics filters [15]. In the optical time domain, the BDG has been excited by the Brillouin interaction between two counter-propagating pump waves, pulsed wave and frequency-downshifted (frequency-upshifted) continuous wave (CW) [16]. In the frequency-downshifted CW configuration, the power of the pump pulse continuously transfers to the frequency-downshifted CW through the SBS effect, which leads to an attenuated BDG along the PMF. By using this scheme, a distributed birefringence measurement of a 500-m PMF was realized [17], which is, to the best of our knowledge, the maximum range of a distributed birefringence measurement of a PMF. Brillouin optical time-domain analysis (BOTDA) using Brillouin loss have been widely used for distributed strain and temperature measurement, which rely on mapping the loss spectrum along the sensing fiber [18]. For a long-range measurement, the loss spectrum at
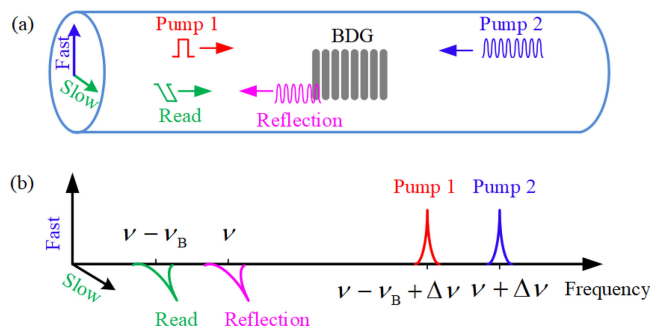
Fig. 1. (Color online) (a) Operation principle of the enhanced BDG. (b) Frequency relationship between pump 1, pump 2, read, and BDG reflection in the enhanced BDG generation and readout processes.

the far end of the fiber will be distorted by the frequency-dependent non-local effect [19]. In the frequency-upshifted CW configuration, an enhanced BDG is generated by the Brillouin interaction between the pump pulse and frequency-upshifted CW, without a frequency sweeping of the pump pulse and CW, which is not limited by the non-local effect.

PMFs have been widely used in fiber optic gyroscopes (FOGs) based on the Sagnac effect of two counter-propagating waves in a fiber coil. It is well known that the polarization nonreciprocal phase error induced by the birefringence change largely reduces the performance of the FOG [20]. A distributed birefringence characterization of the PMF in the fiber coil can provide important information to suppress the polarization nonreciprocal error [21]. However, the 500-m range is not sufficient for the mapping of the birefringence distribution of the fiber coil ($\sim$3000-m PMF) of a high-performance FOG. To extend the measurement range, high-power pump waves are required to increase the intensity of the BDG at the far-end of the PMF. However, the higher-power configuration could lead to nonlinear effects at the far-end of the fiber, such as pump pulse depletion [22], self-phase modulation [23], and modulation instability [24], so that the Brillouin interaction among the two pump waves would be reduced.

In this study, we aim to extend the measurement range of the PMF birefringence based on an enhanced BDG generated by the Brillouin interaction between a pulsed wave and frequency-upshifted CW.

2. Operation Principle

In this section, we present the operation principle of the enhanced BDG (Fig. 1). Two pump waves (optical pulsed pump 1 and CW pump 2) counter-propagate along the fast polarization axis of a PMF, as illustrated in Fig. 1(a). The BDG is excited through the Brillouin interaction of the pump waves when their frequency difference is equal to the Brillouin frequency shift (BFS, υ_B) of the PMF. A read pulse propagating along the slow axis is used to detect the BDG. The maximum reflection would be achieved under the phase-matching condition [12]. The frequency relationship between pump 1, pump 2, read, and reflection in the enhanced BDG generation and readout processes is shown in Fig. 1(b). The lower-frequency pump 1 pulse is continuously amplified by the higher-frequency CW pump 2 through the SBS effect. By utilizing the power of the pulsed pump 1 increasing along the PMF, an enhanced BDG along the PMF can be excited so that an extended measurement range of the BDG reflection spectrum can be realized.

The BDG generation and readout are a Brillouin-enhanced four-wave mixing effect, which can be expressed by [3], [12]

$$\left(\frac{\partial}{\partial z} + \frac{n_f}{c}\frac{\partial}{\partial t}\right)A_1 = ig_0\rho A_2 \tag{1}$$

TABLE 1

Simulation Parameters in the BDG Generation and Readout Processes

Wavelength (nm)	1550
PMF length (m)	3500
Effective mode field (μm^2)	50
SBS gain coefficient (m/W)	5×10^{-11}
Photon lifetime (ns)	10
Slow axis index	1.4689
Fast axis index	1.4683
Peak power of pump 1 (W)	0.5
Power of pump 2 (mW)	0.8
Peak power of read (W)	0.5

$$\left(-\frac{\partial}{\partial z} + \frac{n_f}{c}\frac{\partial}{\partial t}\right) A_2 = ig_0 \rho^* A_1 \tag{2}$$

$$\left(-\frac{\partial}{\partial z} + \frac{n_s}{c}\frac{\partial}{\partial t}\right) A_3 = ig_0 \rho^* A_4 e^{i\Delta kz} \tag{3}$$

$$\left(\frac{\partial}{\partial z} + \frac{n_s}{c}\frac{\partial}{\partial t}\right) A_4 = ig_0 \rho A_3 e^{-i\Delta kz} \tag{4}$$

$$\left(\frac{\partial}{\partial t} + \frac{1}{\tau}\right) \rho = ig_a(A_1 A_2^* + A_3^* A_4 e^{i\Delta kz}) \tag{5}$$

where A_1, A_2, A_3 and A_4 are the optical field amplitudes of pump 1, pump 2, BDG reflection, and read, respectively, ρ describes the acoustic wave, n_f and n_s are the refractive indices along the fiber fast and slow axes, respectively, $g_B = 2g_0 g_a \tau$ is the SBS gain coefficient, τ is the phonon lifetime, c is the light speed in vacuum, and $\Delta k = (k_4 - k_3) - (k_1 - k_2)$ is the phase mismatch.

Further, we investigate the attenuated BDG (i.e. frequency-downshifted CW pump 2) and enhanced BDG (i.e. frequency-upshifted CW pump 2). The simulation parameters in the BDG generation and readout processes is shown in Table 1. In the simulation, the widths of the pump 1 and read pulses are set to 18.5 and 4 ns, respectively. The frequency offset of the two pump waves is set to the BFS of the PMF. The simulation results under the phase-matching condition ($\Delta k = 0$) are shown in Fig. 2, in which the dot- and square-lines correspond to the attenuated and enhanced BDGs, respectively. Fig. 2(a) shows that the Brillouin gain of pump 2 in attenuated BDG decreases along the fiber, while the Brillouin loss of pump 2 in enhanced BDG increases. Fig. 2(b) shows that the power of pump 1 in the attenuated BDG generation has a decreasing trend, while the power of pump 1 in the enhanced BDG generation has an increasing trend. A large depletion of the pump 1 pulse will occurs when a higher-power CW pump 2 is used in the attenuated BDG generation. As shown in Fig. 2(c), the intensity of the attenuated BDG decreases along the fiber, while that of the enhanced BDG increases. Although the power of the BDG reflection is small, $\sim$0.5 μW before 350 m (Fig. 2(d)), it smoothly decreases for the attenuated BDG but largely increases for the enhanced BDG.

3. Experimental Setup

For distributed measurement of BDGs, a general, simplified setup is shown in Fig. 3. A 3030-m-long PMF coil was used as a fiber under test (FUT), which had 64 layers with $\sim$100 turns for each layer. A narrow linewidth distributed-feedback (DFB) laser operating at $\sim$1550 nm was used to provide pump 1 and pump 2. Its output power was split into two branches by a 70/30 coupler (OC).
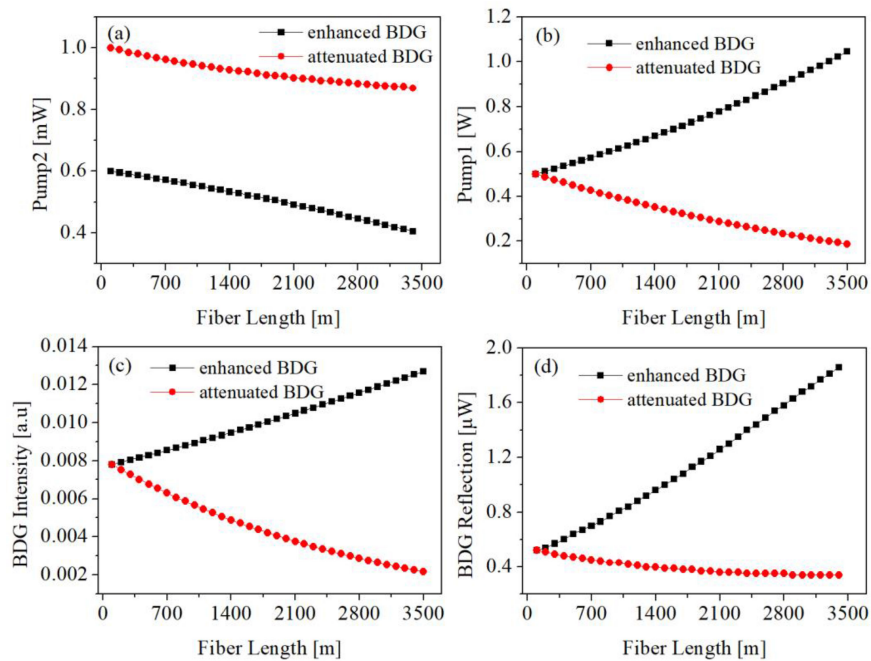
Fig. 2. Simulation results. (a) Pump 2 power, (b) Pump 1 power, (c) BDG intensity, and (d) BDG reflection power as functions of the position along the fiber for the attenuated and enhanced BDGs.
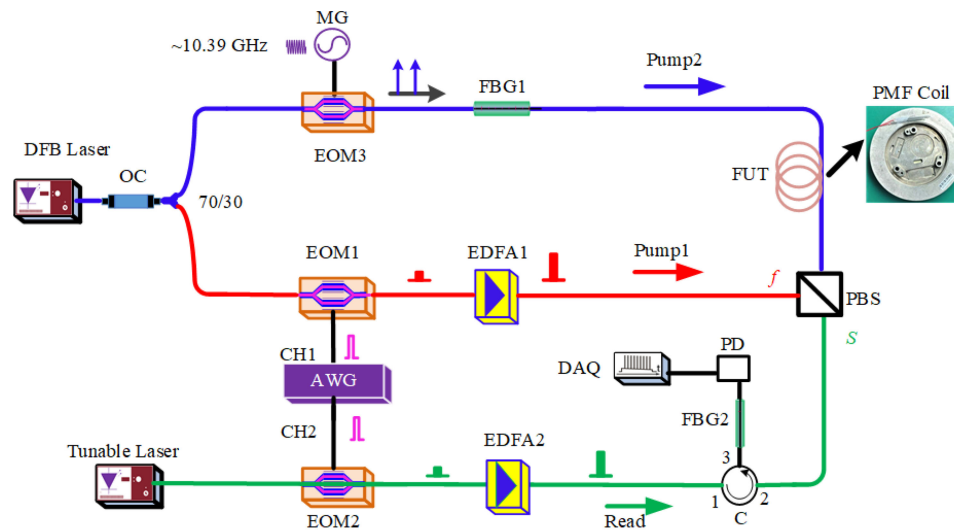

Fig. 3. Experimental setup. C: circulator; DAQ: data acquisition.

The upper branch with the 70%-power component was modulated by an electric-optic modulator (EOM3) driven by a sinusoidal microwave signal output from a microwave generator (MG). Two first-order sidebands were generated by EOM3 by adjusting its operation point with suppressed carrier. The lower- or higher-frequency sideband was selected as CW pump 2 by a fiber Bragg grating (FBG1) by adjusting the operation wavelength of the DFB laser. The CW pump 2 with a power of 0.9 mW was injected along the fast axis of the FUT. The lower branch with the 30%-power component was modulated by EOM1 driven by an electrical pulse output from channel 1 (CH1) of
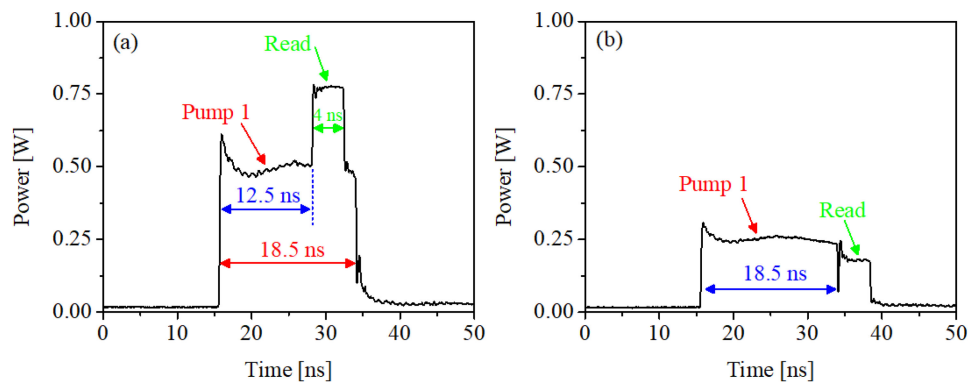
Fig. 4. Time traces of the pump 1 and read pulses at the (a) start and (b) end points of the FUT.

an arbitrary-wave generator (AWG), which led to an 18.5-ns pulsed pump 1 with 0.5-ns rising/falling edges. The peak power of pump 1 was amplified to 0.5 W by an erbium-doped amplifier (EDFA1) and launched along the fast axis of the FUT through a polarization beam splitter (PBS).

A tunable laser with a wavelength resolution of 0.1 pm was used to read the BDG created by the two pump waves. EOM2 driven by the output of channel 2 of the AWG was used to generate a 4-ns read pulse with 0.5-ns rising/falling edges, corresponding to a spatial resolution of 40 cm. The peak power of the read pulse was amplified to 0.3 W by EDFA2. The read pulse was launched along the slow axis through the PBS to read the BDG. The reflection wave of the BDG was detected by a photodetector (PD), before which a fiber Bragg grating (FBG2) with a reflectivity of 97% was used to filter out the cross-talk of pump 2 from the fast axis to the slow axis.

In the experiment, a time delay of 12.5 ns between the pump 1 pulse and read pulse was set at the starting point of the FUT (i.e. the connection point between PBS and FUT), as shown in Fig. 4(a). The time traces of the pump 1 and read pulses at the end of the FUT (i.e. the connection point between FUT and FBG1) are shown in Fig. 4(b). Their time delay increases to 18.5 ns with a variation of 6 ns induced by the group refractive index difference between the fast and slow axes. In addition, the falling edge of the pump 1 pulse meets the rising edge of the probe pulse, which ensures the maximum BDG reflection at the end point of the FUT.

4. Results

In the experiment, the powers of pump 1, pump 2, and read were set to 400, 1, and 300 mW, respectively. The frequency offset between the pump 1 and read pulses was scanned in the range of 71.5 to 74 GHz to obtain the reflection spectrum of the BDG. Top views of the measured three-dimensional (3D) reflection spectra over the FUT (PM1550-80, made by YOFC) of the attenuated and enhanced BDGs are shown in Fig. 5(a) and 5(b), respectively, where the shifts of the BDG reflection spectra are attributed to the birefringence fluctuation over the PMF. Fig. 5(a) shows that the intensity of the reflection spectrum decreases along the PMF and vanishes at the last 500-m PMF, as the transfer of energy from the pump 1 pulse to the frequency-downshifted CW pump 2 occurs continuously so that the intensity of the BDG at the end of the PMF is very small (attenuated BDG). On the contrary, the intensity of the reflection spectrum slowly increases along the PMF, as shown in Fig. 5(b), because the pump 1 pulse is continuously amplified by the frequency-upshifted CW pump 2 (enhanced BDG). However, in a long-range fiber, the intensity of enhanced DBG at the far end of the fiber will be limited by MI effect induced by the excess amplification on pump 1 pulse [23]–[24]. As a result, the intensity of enhanced BDG in a long-range PMF cannot always increase along the distance.
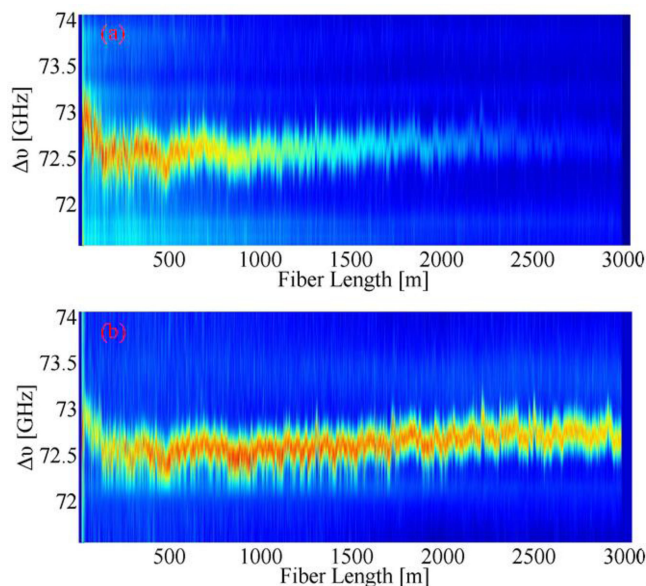
Fig. 5. Measured 3D BDG spectra over the FUT based on the (a) attenuated and (b) enhanced BDGs.
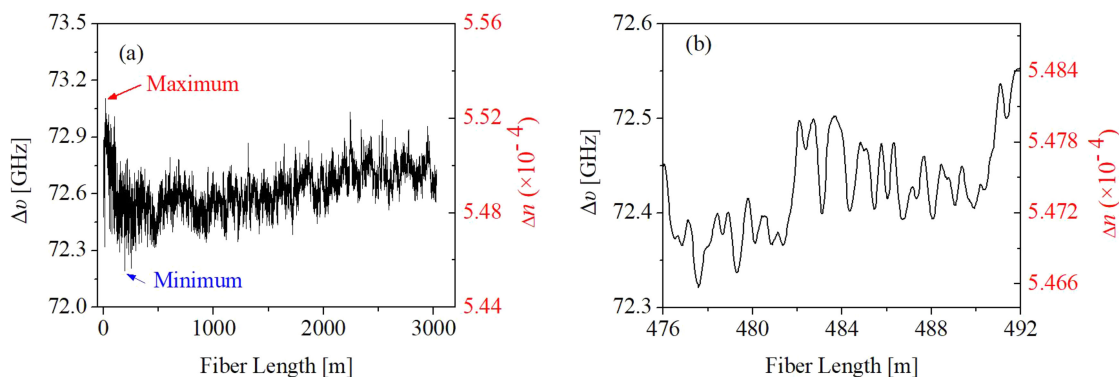

Fig. 6. Calculated birefringence over the (a) entire FUT and (b) segment in the range of 476–492 m.

The center frequency of the reflection spectrum of the BDG, referred to as birefringence-induced frequency shift, is linearly dependent on the local birefringence of the PMF [1]. Based on the reflection spectrum of the enhanced BDG (Fig. 5(b)), the center frequency obtained by Gaussian fit of the BDG spectrum and the calculated birefringence over the PMF are shown in Fig. 6(a). The maximum birefringence is 5.53×10^{-4} at a position of 17.1 m (marked in the figure), while the minimum birefringence is 5.46×10^{-4} at a position of 195.1 m (marked in the figure). The fluctuation of the birefringence over the PMF can be clearly distinguished. It could be caused by the residual stress induced by various disturbance factors during the fiber drawing and coating or uneven stress in the winding of the fiber to the spool. A magnified view of the segment in the range of 476–492 m is presented in Fig. 6(b). We can observe that the change of $\Delta \upsilon$ in the range of a few hundreds of MHz, which should be caused by the uneven stress as winding the PMF to the spool. In the experiment, we use the variation in $\Delta \upsilon$ of ten repeated measurements to characterize the $\Delta \upsilon$ measurement standard deviation. The standard deviation of $\Delta \upsilon$ is ± 22.3 MHz, corresponding to a birefringence measurement accuracy of 1.8×10^{-7}.

5. Conclusion

We have theoretically analyzed and experimentally demonstrated an enhanced BDG through the Brillouin interaction between the pulsed pump 1 and frequency-upshifted CW pump 2, which can be used to realize an extended range of the PMF birefringence measurement. With the 4-ns read pulse corresponding to a spatial resolution of 40 cm, the measurement range of the PMF birefringence was extended to 3030 m, an improvement by a factor of almost 2 compared to the attenuated BDG configuration. By optimizing the parameters of the time delay between the pump 1 and read pulses, optical pulse extinction ratio, and powers of the pump waves, a considerably longer measurement range of the PMF birefringence could be achieved. We believe that the enhanced BDG can be a promising solution to characterize the design of a fiber coil to improve the performance of the FOG.

References

[1] K. Song, W. Zou, Z. He, and K. Hotate, "All-optical dynamic grating generation based on Brillouin scattering in polarization-maintaining fiber," *Opt. Lett.*, vol. 33, no. 9, pp. 926–928, 2008.

[2] Y. Dong, L. Chen, and X. Bao, "Characterization of the Brillouin grating spectra in a polarization-maintaining fiber," *Opt. Express*, vol. 18, no. 18, pp. 18960–18967, 2010.

[3] D. Zhou, Y. Dong, L. Chen, and X. Bao, "Four-wave mixing analysis of Brillouin dynamic grating in a polarization-maintaining fiber: Theory and experiment," *Opt. Express*, vol. 19, no. 21, pp. 20785–20797, 2011.

[4] M. Santagiustina, S. Chin, N. Primerov, L. Ursini, and L. Thevenaz, "All-optical signal processing using dynamic Brillouin gratings," *Sci. Rep.*, vol. 3, 2013, Art. no. 1594.

[5] W. Zou, Z. He, and K. Hotate, "Complete discrimination of strain and temperature using Brillouin frequency shift and birefringence in a polarization-maintaining fiber," *Opt. Express*, Vol. 17, no. 3, pp. 1248–1255, 2009.

[6] F. Li, T. Lan, L. Huang, I. P. Ikechukwu, W. Liu, and T. Zhu, "Spectrum evolution of Rayleigh backscattering in one-dimensional waveguide," *Opto-Electron. Adv.*, vol. 2, 2019, Art. no. 190012.

[7] A. Denisov, M. A. Soto, and L. Thevenaz, "Going beyond 1000000 resolved points in a Brillouin distributed fiber sensor: Theoretical analysis and experimental demonstration," *Light Sci. Appl.*, vol. 5, no. 5, 2016, Art. no. e16074.

[8] Y. Mizuno, N. Hayashi, H. Fukuda, K. Y. Song, and K. Nakamura, "Ultrahigh-speed distributed Brillouin reflectometry," *Light Sci. Appl.*, vol. 5, no. 12, 2016, Art. no. e16184.

[9] D. Zhou *et al.*, "Single-shot BOTDA based on an optical chirp chain probe wave for distributed ultrafast measurement," *Light Sci. Appl.*, vol. 7, no. 1, 2018, Art. no. 32.

[10] Y. Dong *et al.*, "Sub-MHz ultrahigh-resolution optical spectrometry based on Brillouin dynamic gratings," *Opt. Lett.*, vol. 39, no. 10, pp. 2967–2970, 2014.

[11] K. Song, K. Lee, and S. B. Lee, "Tunable optical delays based on Brillouin dynamic grating in optical fibers," *Opt. Express*, vol. 17, no. 12, pp. 10344–10349, 2009.

[12] Y. Dong, L. Chen, and X. Bao, "Truly distributed birefringence measurement of polarization-maintaining fibers based on transient Brillouin grating," *Opt. Lett.*, vol. 35, no. 2, pp. 193–195, 2010.

[13] R. K. Yamashita, Z. He, and K. Hotate, "Spatial resolution improvement in correlation domain distributed measurement of Brillouin grating," *IEEE Photo. Technol. Lett.*, vol. 26, no. 5, pp. 473–476, 2014.

[14] L. Ursini, and M. Santagiustina, "Applications of the dynamic Brillouin gratings to ultrawideband communications," *IEEE Photo. Technol. Lett.*, Vol. 25, no. 14, pp. 1347–1349, 2013.

[15] J. Sancho *et al.*, "Tunable and reconfigurable multi-tap microwave photonic filter based on dynamic Brillouin gratings in fibers," *Opt. Express, vol.* 20, no. 6, pp. 6157–6162, 2012.

[16] K. Song, K. Hotate, W. Zou, and Z. He, "Applications of Brillouin dynamic grating to distributed fiber sensors," *J. Light. Technol.*, vol. 35, no. 16, pp. 3268–3280, 2017.

[17] Y. Dong, H. Zhang, Z. Lu, L. Chen, and X. Bao, "Long-range and high-spatial-resolution distributed birefringence measurement of a polarization-maintaining fiber based on Brillouin dynamic grating," *J. Light. Technol.*, vol. 31, no. 16, pp. 2981–2986, 2013.

[18] X. Bao, J. Dhliwayo, N. Heron, D. J. Webb, and D. A. Jackson, "Experimental and theoretical studies on a distributed temperature sensor based on Brillouin scattering," *J. Light. Technol.*, vol. 13, no. 7, pp. 1340–1348, 1995.

[19] A. D. Lopez, X. A. Vinuesa, A. L. Gil, S. M. Lopez, and M. G. Herraez, "Non-local effects in dual-probe-sideband Brillouin optical time domain analysis," *Opt. Express*, vol. 23, no. 8, pp. 10341–10352, 2015.

[20] R. Luo, Y. Li, S. Deng, D. He, C. Peng, and Z. Li, "Compensation of thermal strain induced polarization nonreciprocity in dual-polarization fiber optic gyroscope," *Opt. Express*, vol. 25, no. 22, pp. 26747–26759, 2017.

[21] X. Xu, X. Pan, and J. Song, "Analysis of sensing coil polarization properties' effect on performance of fiber optical gyroscope," *Appl. Opt.*, vol. 51, no. 5, pp. 621–625, 2012.

[22] L. Thevenaz, S. F. Mafang, and J. Lin, "Effect of pulse depletion in a Brillouin optical time-domain analysis system," *Opt. Express*, vol. 21, no. 12, pp. 14017–14035, 2013.

[23] S. M. Foaleng, F. Barrios, S. Lopez, M. Herraez, and L. Thevenaz, "Detrimental effect of self-phase modulation on the performance of Brillouin distributed fiber sensors," *Opt. Lett.*, vol. 36, no. 2, pp. 97–99, 2011.

[24] M. N. Alahbabi, Y. T. Cho, T. P. Newson, P. C. Wait, and A. H. Hartog, "Influence of modulation instability on distributed optical fiber sensors based on spontaneous Brillouin scattering," *J. Opt. Soc. Am. B*, vol. 21, no. 6, pp. 1156–1160, 2004.